

Influence of PLGA nanoparticles on the deposition of model water-soluble biocompatible polymers by dip coating

Christophe SINTUREL,*¹ Marylène VAYER,¹ Frédéric MAHUT,¹ Franck BONNIER,² Igor CHOURPA,² Emilie MUNNIER²

¹ Interfaces, Confinement, Matériaux et Nanostructures (ICMN), CNRS-Université d'Orléans, UMR 7374, 1b, Rue de la Férollerie, C.S. 40059, 45071 Orléans Cedex 2, France

² EA 6295 Nanomédicaments et Nanosondes (NMNS), Université de Tours, Faculté de Pharmacie, 31 avenue Monge, 37200 Tours, France

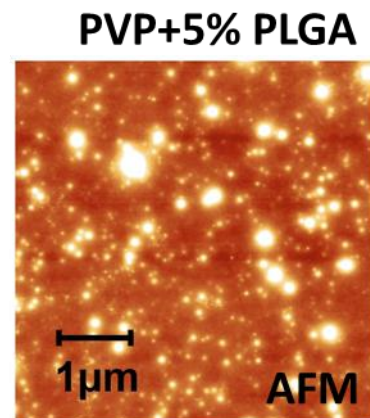
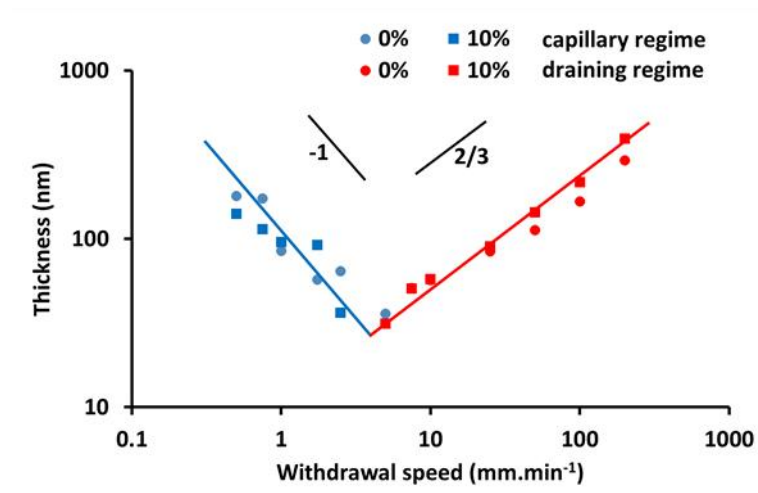
*corresponding author: christophe.sinturel@univ-orleans.fr

Keywords: colloids, water-soluble biocompatible polymer, nanocomposite thin films, dip coating, AFM.

Highlights:

- Thin films of biocompatible polymer loaded with nanoparticles were prepared by dip coating
- Thicknesses of the PVP and PVA films are not affected by the PLGA nanoparticles
- Crystallization of PVA occurs whereas amorphous PVP was obtained
- PLGA nanoparticles are incorporated over the whole range of withdrawal speeds
- The nanoparticle concentration in the film is influenced by the deposition regime

Graphical abstract:



Abstract

This work relies on the use of dip-coating at various withdrawal speeds to form nanocomposite films, with a detailed analysis of the influence of the mode of deposition on the nanoparticle (NP) concentration in the dried film. While the deposition of polymer solutions on the one hand and colloidal suspensions of NPs on the other hand have been separately studied by dip coating, their combination is far being a simple superposition of the two separate behaviors. The formation of nanocomposite thin films composed of model water-soluble biocompatible polymers (polyvinyl alcohol - PVA and polyvinylpyrrolidone - PVP) loaded with poly(lactic-co-glycolic acid) (PLGA) nanoparticles (NPs) was studied through a dip coating process. Flat silicon substrates were removed at a controlled withdrawal speed from an aqueous colloidal suspension. Thin films of PLGA NPs with concentrations ranging from 1 to 10 % wt./wt. in PVA or PVP matrices were prepared. The presence of nanoparticles on the well-established process of thin film deposition was examined, as well as the influence of the deposition regime on the nanoparticle concentration in the deposited coating. We demonstrate that the presence of colloidal dispersion of PLGA nanoparticles in water solution of PVA and PVP does not modify the process of film deposition by dip coating. A typical “V” shaped curve was observed, with two well-known deposition regimes: capillary and draining modes respectively obtained at low and high withdrawal speeds. Due to crystallization at low withdrawal speed (favored by slow evaporation of the solvent) it was not possible to identify individual PLGA nanoparticles by AFM in the case of the PVA matrix. Amorphous PVP nanocomposite films were successfully prepared by dip coating, and allowed us to identify individual PLGA nanoparticles with AFM. Because of the prevalence of an evaporation-driven phenomenon at low withdrawal speed, incorporation of NPs was observed over the whole range of withdrawal speeds, showing original behavior compared to recent studies relying on a pure Landau-Levich regime (i.e. non-evaporative

systems). Our results indicate that the nanoparticles were not equally retrieved from the solution in the capillary and the draining regime. This suggests that the balance between the viscous drag and the interfacial effects depends on the deposition mode and calls for a more detailed analysis of the physical processes involved in both regimes.

Introduction

In nanocomposite materials, the small volume of nanoscale fillers induces specific behavior in comparison to their macro-scale counterparts, such as an extremely high surface-to-volume ratio or improved chemophysical responsiveness. Given that the intrinsic properties of the nanofillers in the coating differ strongly from the bulk due to confinement effects arising from the limited amount of matter, the elaboration of nanocomposites has attracted a great deal of interest over the last decades.^{1,2} More specifically, nanocomposite materials in the form of films or coatings have found outstanding applications in packaging,^{3,4} sensors⁵, and membranes^{6,7} thanks to improved mechanical⁸, dielectric,⁹ antibacterial,¹⁰ antifouling,¹¹ permeability¹² or optical properties.¹³ Drug delivery from nanocomposite coating has also emerged as a strategy to improve the integration of biomedical materials in the body and increase their efficiency through local drug release.^{14,15,16} In this field, innovation is high. Triggerable drug delivery using nanocomposite coatings has for example recently emerged.¹⁷ In this case, the inclusion of nanofillers renders matrices responsive to external stimuli, increasing their tunability and responsiveness in terms of drug release.

Among the various methods used to deposit surface layers, dip coating is a very simple way for coating objects, even with more complex shapes than flat surfaces, such as fibers^{18,19,20} that could find valuable applications in the field of biomedical implants²¹. It consists in dipping the substrate into a solution containing the material to be deposited, and withdrawing the substrate at a constant speed. The process can be automated and can therefore be easily implemented in industrial processes, on any type of materials or objects.²² Depending on the withdrawal speed, the nature of the solvent, and the concentration of the solvent vapors above the reservoir, the thickness of the coating can be finely tuned. Dip coating was first studied in the case of a non-evaporative liquid in the pioneering work of Landau and Levich²³. It has been extended to sol-gel processes,^{24, 25} and polymer solutions,^{26,27} where, as the solvent

evaporates, it has been demonstrated that deposition occurs in two specific regimes, namely the capillary and the draining regimes (for low and high withdrawal speeds respectively). The physical processes of film formation in these two regimes are different (convective and Landau-Levich deposition respectively),²² leading to a typical “V” shaped thickness evolution.²⁸ By extension, the preparation of nanocomposite coatings using dip coating can be easily carried out if the polymer solution contains a colloidal dispersion of nanoparticles (NPs). Polymer and nanoparticles are both retrieved with the solution by the moving substrate, leaving a nanocomposite film after drying. One important question at this stage is whether the presence of nanoparticles can modify the well-established process of thin film deposition and whether NP concentration in the deposited coating can be influenced by the withdrawal speed. In a similar mode of deposition, it has been indeed shown that the deposition of colloidal dispersion in the evaporative regime was strongly influenced by the vapor mass transfer during drying, leading to a deviation of the withdrawal speed dependence of the thickness.²⁹ In addition, it is known that enrichment in nanoparticles can occur at the receding meniscus, similarly to the “coffee ring effect”,^{30,31} leading to a modification of the NP concentration in the dried film, in comparison to the solution.^{32,33} On the contrary, it has been recently shown that a selection of nanoparticules can occur at a low withdrawal speed,³⁴ eventually leading to a situation where only the liquid is entrained, the particles being trapped in the meniscus and left in the bath (capillary filtering)³⁵.

A literature survey shows that despite an abundant number of studies on the use of dip-coating for the deposition of polymer solutions on the one hand and colloidal suspensions of NPs on the other hand, the deposition of more complex systems combining polymer and NPs is much less well documented. Although some studies describe the preparation of nanocomposites by dip-coating,^{36,37,38} no systematic analysis of the deposition process (withdrawal speed, NP concentration, polymer type, etc.) of a polymer solution containing a colloidal suspension of

nanoparticles has been reported to our knowledge. In the present work, we focused on two model biocompatible water-soluble polymers, namely polyvinyl alcohol (PVA) and polyvinylpyrrolidone (PVP) for which we evaluated the effect of the presence of poly(lactic-co-glycolic acid) (PLGA) nanoparticles (a typical carrier for drug encapsulation^{39,40,41}) at moderate concentrations (up to 10%) on the deposition mechanism.

Material and methods

Material

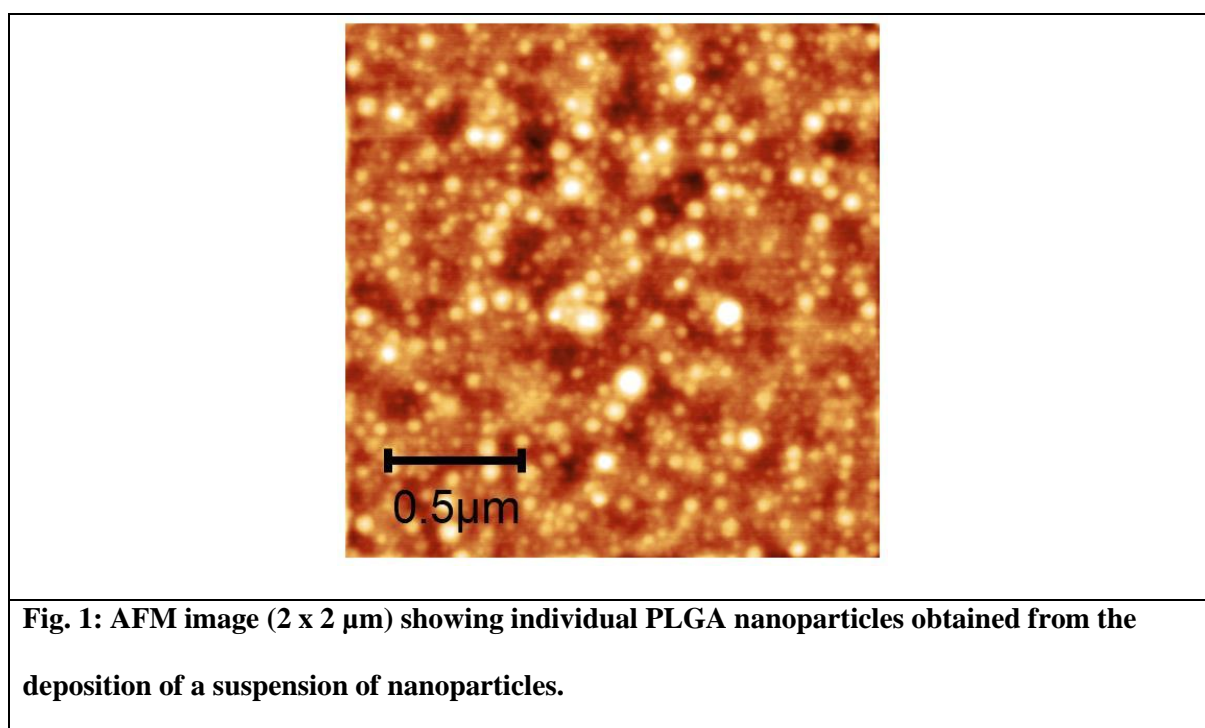
Two polymer matrices (Polyvinyl alcohol (PVA) M_w : 50 kg.mol⁻¹, hydrolysed 87 – 89% from Aldrich, and Polyvinylpyrrolidone (PVP) M_w average: 58 kg.mol⁻¹ from Alfa-Aesar) were used. Distilled water was used as solvent to solubilize these polymers. Poly (lactic – co-glycolic acid) 50:50, mol wt 30,000-60,000, and dimethyl carbonate were purchased from Sigma-Aldrich. Water was purified with a Milli-Q system (Millipore, France).

PLGA nanoparticle preparation and purification

PLGA nanoparticles were prepared by the single emulsion–solvent evaporation process.⁴² To prepare the organic phase, 400 mg of PLGA were dissolved in 4 mL of dimethyl carbonate. The aqueous phase was a PVA solution at 4% wt./wt. at 4°C. The aqueous phase was placed in a cooling Rosett cell in an ice bath. The organic phase was injected in the aqueous phase under ultrasound (20 kHz; Vibra-cell ultrasonic processor, Sonics & Materials, USA). Sonication was continued during 2 minutes. Then, the dimethyl carbonate was evaporated under vacuum at 40°C, 50 mbar for 30 minutes (Welch ILMVEC, USA). Samples were then centrifuged (15000xg, 20 min) and the supernatant was discarded. The pellets were dispersed in 10 mL of ultrapure water and centrifugation was repeated to purify the sample from the excess of surfactant. The pellet was finally dispersed in 10 mL of ultrapure water and stored at 4°C. The NP concentration in the final suspension was 13 mg.mL⁻¹.

Nanoparticle characterization

The nanoparticle size obtained after deposition of the nanoparticle suspension onto a silicon wafer and evaporation of the solvent was measured by Atomic Force microscopy (AFM, Dimension Icon with ScanAsyst, Bruker, USA). A typical AFM image of deposited nanoparticles is shown in Figure 1. From a systematic analysis of the nanoparticle size performed on a 2 x 2 μm AFM image, a mean size of 45 ± 10 nm was found.



Thin film preparation and characterization

Nanocomposite polymer thin films were prepared from polymer solutions in water, to which a colloidal suspension of PLGA nanoparticles was added. The PVA was solubilized in water by heating (90°C) under magnetic stirring for 2h while the PVP solution was prepared by mixing the polymer and water at room temperature, under magnetic stirring for 1h. The concentration of both PVA and PVP in water was 30 mg.mL^{-1} . Specific amounts of aqueous suspension of PLGA nanoparticles (13 mg.mL^{-1} , 1.3% wt./vol.) were added to the polymer solution (30 mg.mL^{-1} , 3% wt./vol.) in order to get a concentration of PLGA nanoparticles in the dried film

between 1 and 10 % wt./wt. The concentration of solid material in the solution after mixing the two parent solutions was therefore <3% and thus can be considered as a dilute solution. The viscosity of the solution was measured by a DV2T LV viscometer from AMETEK Brookfield (Middleboro, USA). Thin films of polymers were prepared on a silicon substrate by dip coating (dip coater QPI-168, Qualitech Industrial Products, India). The substrate was immersed in the solution (7 mL) at 200 mm.min⁻¹, left in the solution for 1 min and withdrawn at a speed from 0.05 to 200 mm.min⁻¹ depending on the samples. After complete evaporation of the water, dried nanocomposite thin films on silicon were obtained. The thickness of the films was measured by visible reflectometry (F20 Film Thickness Measurement System, Filmetrics, KLA-Tencor, USA). The thicknesses of the films were measured at more than 5 different places and the averaged thicknesses and standard deviations were calculated. For all the films, these standard deviations were less than 10%.

AFM (Dimension Icon with ScanAsyst, Bruker, USA) in tapping mode was performed in order to monitor the different surface topographies depending on the nanocomposite film composition. The surface roughness R was extracted from the AFM image. R represents the amplitude of the deviations (z) of surface heights from the mean height and was estimated by means of the Root Mean Squared (RMS) roughness using the formula where n is the number of heights considered:

$$R = \sqrt{\frac{1}{n} \sum_{i=1}^{i=n} z_i^2}$$

Results and discussion

PVA/PLGA nanocomposite thin films

Figure 2 shows the typical variation of the polymer film thickness (after drying) as a function of the withdrawal speed. The results shown here were obtained with neat PVA and blends of PVA/PLGA NP (5%), deposited by dip coating from solutions in water. In a log/log scale, the thickness versus the withdrawal speed exhibits a typical “V” shaped curve. It first linearly decreases with increasing speed, goes through a minimal thickness for a critical speed, and then linearly increases for higher values of the speed. This is consistent with the expression of the thickness (h_f) versus the withdrawal speed (U_0) which, in the case of a dried film formed upon solvent evaporation, can be written as follows (equation 1):²⁴

$$(Eq\ 1.)\ h_f = k_i \left(\frac{E}{L} \frac{1}{U_0} + D U_0^{2/3} \right)$$

where k_i depends on the mass concentration of the polymer in the solution (c_i in $g.cm^{-3}$) and the density of the polymer (ρ_i in $g.cm^{-3}$) by $k_i = c_i / \rho_i$. E , L , D are the evaporation speed, the film width and the global draining constant respectively. In our case, k_i was $2.5 \cdot 10^{-5}$ and L was 0.01 m.

As seen from this expression, the thickness is proportional to the inverse of the speed at low withdrawal speed and proportional to $2/3$ of the withdrawal speed at high withdrawal speed. These two stages correspond to the so-called “capillary” and “draining” regimes respectively (represented in blue and red for better clarity on Figure 2), and are clearly verified in our results with a slope in log-log scale of -1 for the low withdrawal speeds and $2/3$ for the high withdrawal speeds. These two regimes result from different physical processes that dominate as a function of the withdrawal speed.^{43,44} In brief, the formation of higher thicknesses is favored at low speed due to a continuous capillary flow that drags the solution towards the film in formation, upon an evaporation-driven phenomenon. In contrast, higher film

thicknesses are built-up above the critical speed due a direct increase in the amount of solution removed by the withdrawn substrate, resulting from the interplay between the viscous drag of the solution and surface tension (described by the Landau-Levich equation²³). The superposition of the curves for the neat polymer and the nanocomposite thin film shows that PLGA nanoparticles do not significantly modify the deposition process of PVA film, whether in the draining or the capillary regime. From a fit of the linear parts with Eq. 1, E and D were estimated respectively at $4 \cdot 10^{-13} \text{ m}^3 \cdot \text{s}^{-1}$ and $3 \cdot 10^{-4} \text{ m}^{1/3} \cdot \text{s}^{2/3}$ for both neat PVA and the blend PVA/PLGA NP (5%). These values are in the range of the values obtained in previous work²⁷ showing similar values of D for polymer solutions loaded at $30 \text{ mg} \cdot \text{mL}^{-1}$ (the same concentration as in the present study) but higher values of E since the solutions were obtained in organic solvent having a much faster evaporation rate.

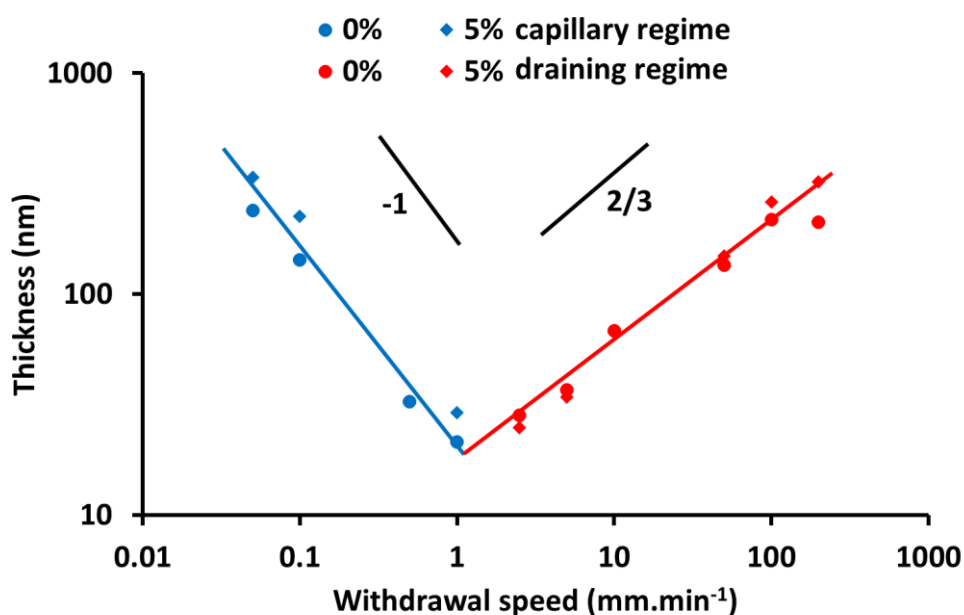


Fig. 2: Influence of PLGA nanoparticle concentration on the thickness of PVA films obtained by dip coating as a function of the withdrawal speed. Black lines follow slopes of -1 and 2/3 in log-log scale as a guide for the eyes. The standard deviation on each experimental point is 10%.

Since distinct physical processes drive the formation of the films in the “capillary” and the “draining” regimes, the question that arises is whether or not the withdrawal speed affects the composition of the film (i.e. the NP concentration in the final film). From the applications standpoint mentioned in the introduction, such as drug delivery, this is a crucial aspect since it can lead to enrichment or depletion of the NPs in the film. In order to evaluate the NP concentration in the film, we carried out AFM analysis of the surface of the film. Because the NP size (45 nm) is not negligible compared to the film thickness (20 to 200 nm), we anticipated that embedded NPs could be identified by AFM.

Figure 3 shows the surface topographies of the neat PVA (left) and PVA/PLGA NP (5%) blend (right) obtained by AFM, for three distinct deposition behaviors: in the capillary regime (a), in the intermediate regime (b) and in the draining regime (c). More images are shown in the supporting information (Figure SI-1). At high withdrawal speed (c), neat PVA displays a smooth uniform surface with low RMS roughness (0.6 nm at $200 \text{ mm} \cdot \text{min}^{-1}$). In contrast, the PVA/PLGA NP (5%) blend displays white spots on the surface that can be attributed to embedded nanoparticles, exhibiting higher RMS roughness (1.6 nm at $200 \text{ mm} \cdot \text{min}^{-1}$). From a systematic analysis of the AFM images, we found an average feature size of $51 \pm 11 \text{ nm}$, in good agreement with the size of the NPs (see experimental part). The increased diameter of the NPs in the film can be attributed to a PVA coating of the PLGA NPs. At low withdrawal rate (Figure 3 a)) the topography is very different. Both systems (PVA and PVA/PLGA NP (5%) blend) exhibit a very rough surface with a RMS roughness respectively of 13.4 and 10.1 nm, with strong local variations of the z profile (as shown in the insert). This phenomenon can be attributed to a crystallization of the polymer, which dominates the surface roughness. In previous work, we showed that withdrawal speed has a significant impact on the crystallization of polymers,⁴⁵ which in turn greatly affects the surface roughness. We demonstrated that the crystallization process was favored at low withdrawal speed, where the

slow solvent evaporation allows for the nucleation and growth of the crystalline domains. In contrast, the high evaporation that occurs at higher withdrawal speeds acts as a quench, and favors the formation of an amorphous phase. In the present case, it is well known that PVA is a semi-crystalline polymer, even in its atactic form (which can crystallize up to 65%).⁴⁶ This was confirmed by DSC which shows a strong exothermal signal while heating (see Figure SI-2). As a result, the surface topography is dominated by the formation of crystalline features at low withdrawal speed, preventing the observation of the particles in the nanocomposite films. The particle amount as a function of the deposition rate is consequently not accessible. After observing this behavior, we therefore did not conduct a detailed NP concentration analysis of the surface topography and we switched to a fully amorphous system, PVP, which is now described.

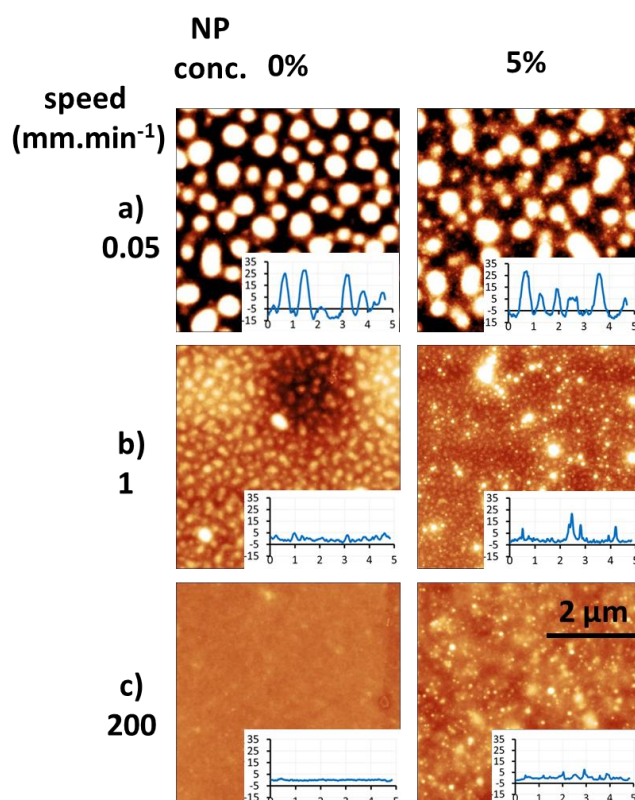


Fig. 3: Influence of PLGA nanoparticle concentration and withdrawal speed on the morphology of PVA thin films investigated by AFM. a) 0.05 mm.min⁻¹ in the capillary

regime b) 1 mm.min⁻¹ in the intermediate regime c) 200 mm.min⁻¹ in the draining regime. The inserts show typical topographical cross sections of AFM images. All images are 5*5 μm , Z scale= ± 10 nm.

PVP/PLGA nanocomposite thin films

In order to cope with the crystallization process observed in the case of the PVA films formed at low withdrawal speed, we moved to the formation of nanocomposite thin films using PVP, a fully amorphous polymer. Both the film thickness and NP concentration were studied with respect to the withdrawal speed, on a range of PLGA NP concentration spanning from 1 to 10%.

Figure 4 shows a typical variation of the polymer film thickness as a function of the withdrawal speed, for the neat PVP and nanocomposite thin film. Similarly to the PVA case, the NPs do not significantly modify the thickness of the PVP film, over the range of NP concentration explored in this study, whether in the capillary or the draining regime. All the thickness curves are superimposed onto a single master curve. As for the PVA case, the values of E ($1 \cdot 10^{-11} \text{ m}^3 \cdot \text{s}^{-1}$) and D ($3 \cdot 10^{-4} \text{ m}^{1/3} \cdot \text{s}^{2/3}$) were extracted from a fit of the linear parts with equation Eq. 1. The difference between the E values for PVA ($4 \cdot 10^{-13} \text{ m}^3 \cdot \text{s}^{-1}$) and PVP ($1 \cdot 10^{-11} \text{ m}^3 \cdot \text{s}^{-1}$) can be attributed to the better affinity of PVA compared to PVP towards water.²⁷ In contrast, the value of D does not differ for the solutions of PVA and PVP and is not affected by the NP concentration. This suggests that the viscosity of the solutions is not affected in our case by the nature of the polymer, nor the NP concentration. This was verified by measuring the viscosity of the solutions which was found to be constant (1.13 mPa.s) and relatively close to the viscosity of water (0.90 mPa.s). This is in good agreement with the fact that all solutions contained a limited amount of solid material (< 3%). This case is quite

different from the work of Gans and coworkers⁴⁷, where the solid content in solution was between 10 and 41%, with a dramatic impact on the viscosity.

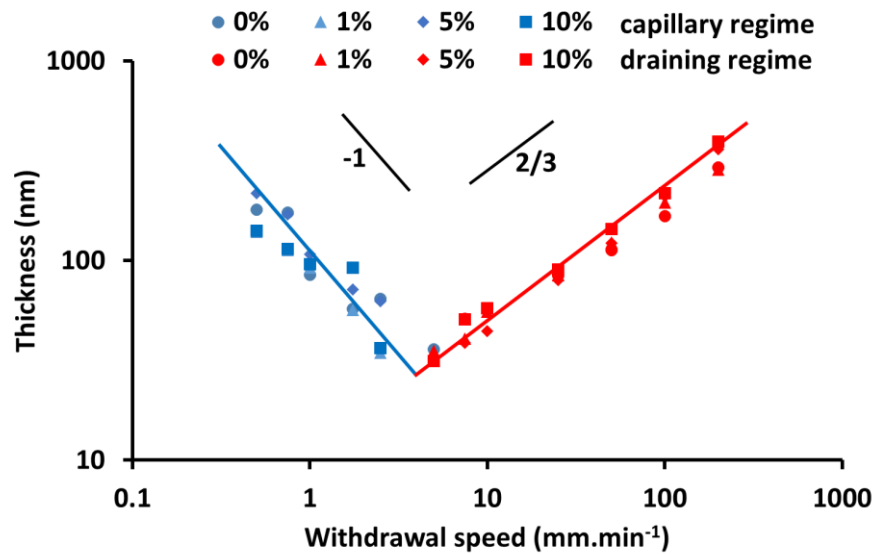


Fig. 4: Influence of PLGA nanoparticle concentration on the thickness of PVP films obtained by dip coating as a function of the withdrawal speed. Black lines follow slopes of -1 and 2/3 in log-log scale as a guide for the eyes. The standard deviation on each experimental point is 10%.

Figure 5 displays the surface observations of films obtained using three representative conditions of the withdrawal speed (0.5 mm.min⁻¹ in the capillary regime, 10 mm.min⁻¹ near the critical point and 200 mm.min⁻¹ in the draining regime), as a function of the NP concentration. On the neat PVP film, the surface of the film remained perfectly smooth whatever the withdrawal speed, indicating that no crystallization occurred upon drying. This is consistent with the structure of PVP that exhibits an amorphous behavior, which was confirmed by DSC (see Figure SI-3). Consequently, the modification in the film topography can be solely attributed to the presence of the PLGA nanoparticles, which appear as white spots on the surface (with dimensions in good agreement with the NP size) in both the capillary and the draining regime. In this case, the systematic analysis of the AFM images

gives an average feature size of 58 ± 15 nm. Again, the increased diameter of the NPs in the film can be attributed to a PVP coating.

Unlike PVA, PVP-based nanocomposite films can be used to evaluate the influence of the deposition mechanisms on the incorporation of the NPs in the films. For that purpose, instead of a direct, time-consuming counting of NPs on the AFM images (which cannot be automated due to complex threshold adjustments), we used the film roughness as an indicator of the NP concentration in the film. As all the images are at the same z-scale, one can directly compare the different conditions. Clearly, the intermediate withdrawal speed leads to higher roughness. However, it does not mean that the number of PLGA nanoparticles is higher. One has to keep in mind that the thickness depends on the withdrawal speed. At $10 \text{ mm} \cdot \text{min}^{-1}$, the thickness of the film is minimal (c.a. 35 nm), and is thinner than the size of the nanoparticles. This makes the nanoparticles clearly visible on the AFM images, in contrast to the thicker films where the nanoparticles are embedded in the polymer matrix, leading to a smoother appearance of the surface. This clearly indicates that the roughness of the films cannot be used to compare the NP concentration between two films of different thicknesses. However, for two films having the same thickness, but obtained in two deposition regimes, the roughness extracted from the AFM images can be used to conclude on the influence of the deposition regime on the amount of NPs in the film.

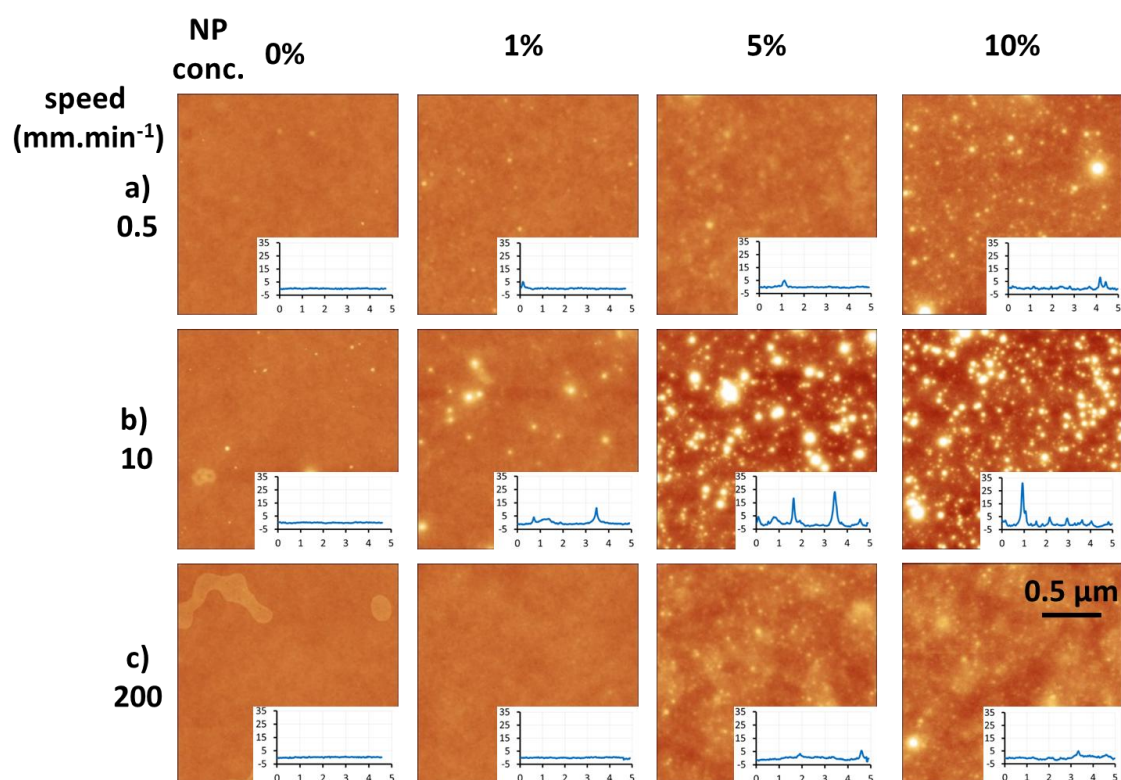


Fig. 5: Influence of PLGA nanoparticle concentration on the morphology of PVP films in three representative conditions of the withdrawal speed: a) 0.5 mm.min⁻¹ in the capillary regime b) 10 mm.min⁻¹ near the critical point c) 200 mm.min⁻¹ in the draining regime. The size of the AFM images is 2*2 μm. Z scale=±10 nm. The inserts show typical topographical cross sections of AFM images.

Figure 6 shows the thickness dependence of the thin film roughness, in the two deposition regimes (draining in red and capillary in blue). For the neat polymer, the roughness is almost constant (0.2 nm) with the film thickness indicating that the deposition regime (draining or capillary) has no influence. For the nanocomposite films, the roughness is maximum for the smallest value of film thickness (~35 nm), and decreases for higher thickness values, eventually reaching a plateau, in a similar way for both the capillary and draining regimes. As previously mentioned, this phenomenon mostly originates from a scale difference between the nanoparticle diameter and the PVP thickness: the NPs become more deeply buried in the film

as the thickness increases, resulting in the observed decrease in roughness (a plateau is reached when the thickness of the film becomes similar to or higher than the NP size, c.a. 50 nm). As previously mentioned, the roughness variation between films of different thicknesses is not an indication of the NP concentration in the dried film. However, if one considers a similar film thickness, the roughness values can be used as qualitative information to compare the concentration of nanoparticles in the dried films: a low concentration leads to low roughness, and a higher concentration to higher roughness.

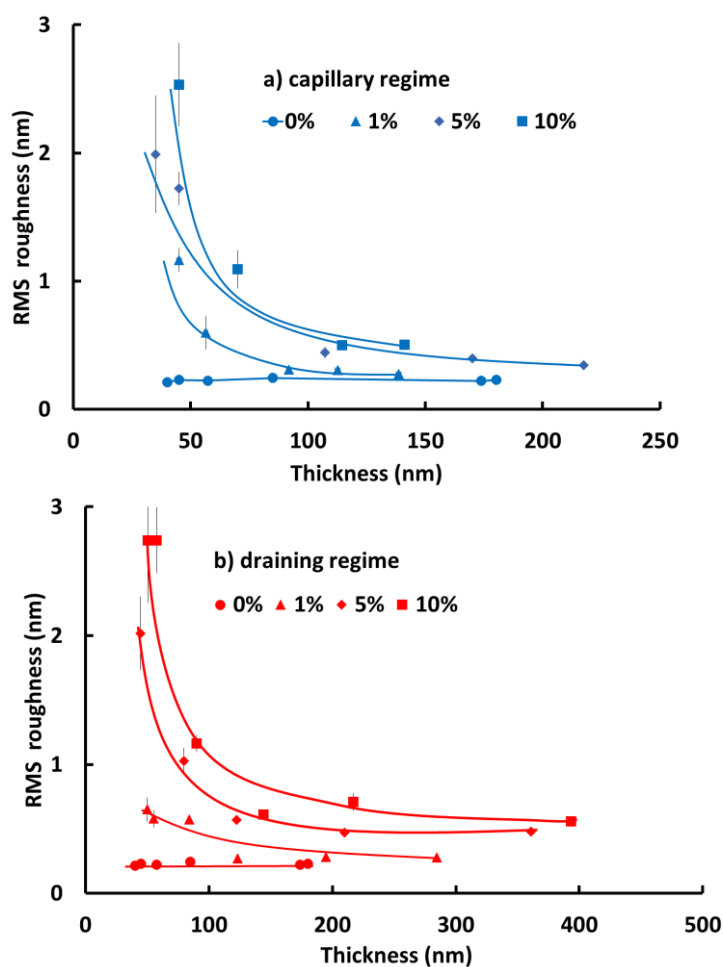


Fig. 6. Variation of the film roughness in the capillary regime (a) and the draining regime (b) as a function of the film thickness for different concentrations of NP. The standard deviation on each experimental point is shown as a black vertical line.

To gain greater insight into the influence of this property, Figure 7 shows the roughness level observed for films at 50 nm. A lower roughness value is observed in the capillary regime, indicating a depleted NP concentration in the dried film and consequently suggesting that NP entrainment is influenced by the deposition mode in this case. This was confirmed by an individual counting of the NPs on 3 different $2 \times 2 \mu\text{m}$ scale images (more than 300 measurements). 25 NPs. μm^{-2} were found in the draining regime, versus 18 NPs. μm^{-2} in the capillary regime, confirming a depletion of NPs in the capillary regime (to be compared to the theoretical value of 25 NPs. μm^{-2} calculated with nanoparticles having a diameter of 50 nm, loaded at 5 % in a film).

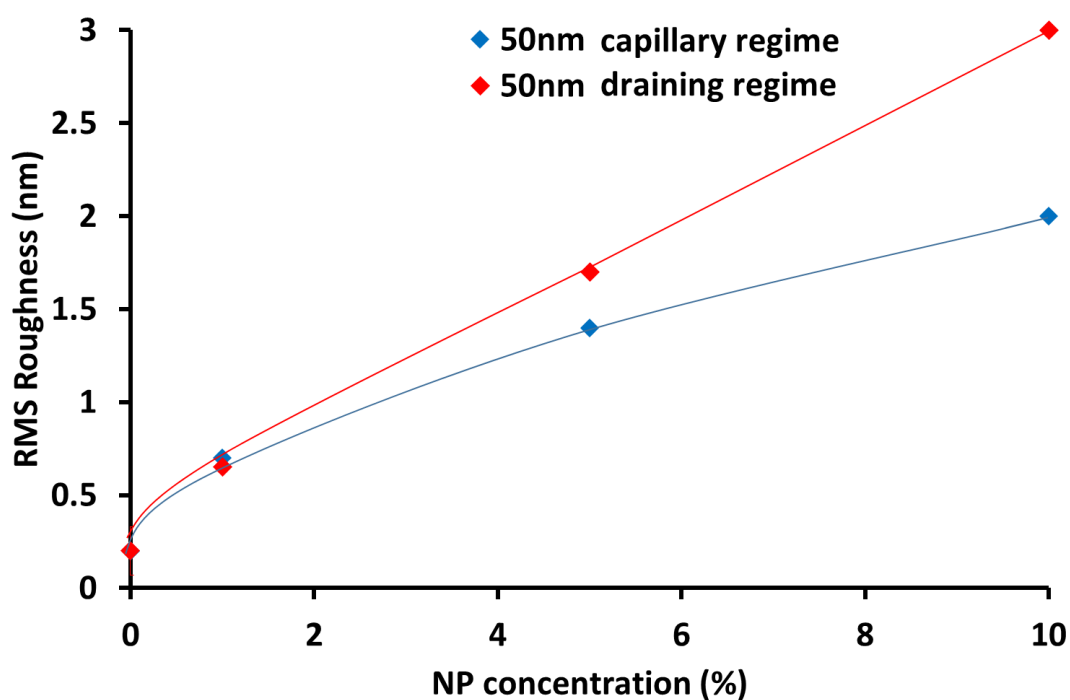


Fig. 7. Variation of the film roughness at 50 nm in the capillary and draining regimes, for different NP concentrations

These results can be analyzed in light of the very recent works by Dincau³⁴ and Sauret³⁵ studying the deposition of particles from a liquid suspension in dip coating. As described by these authors, the NP entrainment by a moving substrate in such a situation results from the competition of two opposite forces. On the one hand, the viscous forces are responsible for retrieving the NPs out of the solution whereas on the other hand the capillary forces tend to curb the meniscus deformation, preventing the NPs from being incorporated in the film. NPs are thus incorporated in the deposited films when the viscous drag overcomes the capillary forces, which is obtained for capillary numbers greater than a critical value that depends mainly on the viscosity of the solution, the NP size and the withdrawal speed. For a given viscosity and NP size, NPs are entrained at high withdrawal speed because of viscous drag. In contrast, NPs incorporation in the film decreases at low withdrawal speed because the capillary forces dominate and may even lead to the point that no particle is found in the film, as shown by Dincau et al.³⁴ and Sauret et al.³⁵. In their situation, such a phenomenon relied on a pure Landau-Levich regime (i.e. without solvent evaporation - the particles are dispersed in non-volatile oil) over the whole range of withdrawal speed values.

In our results, NPs are embedded in the films whatever the withdrawal speed. This is because in our case, the liquid phase evaporates during deposition which leads, in the low withdrawal speed range, to an increase in thickness. This specific effect originates from a self-initiated continuous capillary flow that drags the solution towards the film in formation, in an evaporation-driven phenomenon (similar to the coffee ring effect). Consequently, the NPs are submitted to the same antagonist effects described for the draining regime (viscous vs interfacial forces) that allow for the incorporation of the NPs in the film in our case.

Interestingly, our results suggest that the balance of these two effects is not equivalent in the draining and capillary regime. The underlying physical origin of this phenomenon is currently under investigation.

Conclusion

We showed that the presence of colloidal dispersion of PLGA nanoparticles in a water solution of PVA and PVP does not modify the general process of film deposition by dip coating. A typical “V” shaped curve is observed with two well-known deposition regimes: capillary and draining modes respectively obtained at low and high withdrawal speeds. For both polymer matrices, the thickness is independent of the NP concentration (up to 10%). However, a close look at the coating topographies allowed us to point out differences in the capillary and the draining regimes for both matrices. In the case of the PVA, crystallization was observed at low withdrawal speeds, which is explained by the slow evaporation of the solvent. It was not possible to identify individual PLGA nanoparticles by AFM in this case due to the high surface roughness generated by the crystallization process. In contrast, amorphous PVP nanocomposite films were successfully prepared over the whole range of withdrawal speeds, and allowed us to identify individual PLGA nanoparticles with AFM. When the thickness is sufficiently low, the particles’ presence modifies the topography on the surface and in this case, the roughness measured by AFM was correlated to the NP concentration in the film. Because of the prevalence of an evaporation-driven phenomenon at low withdrawal speed, incorporation of NPs was observed over the whole range of withdrawal speeds, in contrast to other studies relying on a pure Landau-Levich regime (i.e. non-evaporative systems). Our results indicate that the balance between the viscous drag and the interfacial effects depends on the deposition regime and call for a more detailed analysis of the physical processes involved in both regimes. In comparison to the existing literature on the dip-coating deposition of polymer solutions on the one hand and colloidal suspensions on the other hand, this work offers a new perspective. It brings new insights into the influence of NPs on the deposition of polymer solutions by dip-coating (and vice-versa), building essential knowledge dealing with phenomena occurring during the deposition. Combining these two

systems allowed us to reveal new behavior, particularly concerning the incorporation of NPs at low withdrawal speed, making this work particularly relevant, relative to prior literature on the separate systems. From the application standpoint (such as the formation of nanocomposite coatings containing NPs for controlled drug delivery), this work demonstrated that it is important to consider the withdrawal speed for these two major biocompatible polymer models. In the case PVA, crystallinity will greatly depend on the process. In the case of PVP, the NP concentration in the dried film is affected by the mode of deposition.

Acknowledgements

We thank the Région Centre-Val de Loire for funding (MISTIC project ARD 2020 Cosmétosciences 2017-00118114 and Fonds Européen de Développement Régional 2017-EX003256).

References

- ¹ J. Kao, K. Thorkelsson, P. Bai, B. J. Rancatore, T. Xu Toward functional nanocomposites: taking the best of nanoparticles, polymers, and small molecules, *Chem. Soc. Rev.*, 2013, 42, 2654-2678 <https://doi.org/10.1039/C2CS35375J>
- ² S.K. Kumar, B. C. Benicewicz, R.A. VaiaKaren, I. Winey 50th Anniversary Perspective : Are Polymer Nanocomposites Practical for Applications?, *Macromolecules* 2017, 50, 714-731 <https://pubs.acs.org/doi/abs/10.1021/acs.macromol.6b02330>
- ³ R.Q. Assis, S.M. Lopes, T.M.H. Costa, S.H. Flôres A.O. Rios, Active biodegradable cassava starch films incorporated lycopene nanocapsules, *Ind. Crops Prod.* 2017, 109, 818-827 <https://pubag.nal.usda.gov/catalog/5844502>
- ⁴ J.W. Rhim, H.M. Park, C.S. Ha Bio-nanocomposites for food packaging applications, *Prog Polym Sci* 2013, 38, 10-11, 1629-1652 <https://doi.org/10.1016/j.progpolymsci.2013.05.008>
- ⁵ V.E. Bochenkov, N. Stephan, L. Brehmer, V.V. Zagorskii, G.B. Sergeev Sensor activity of thin polymer films containing lead nanoparticles, *Colloids Surf., A*, 2002, 198-200, 911-915 [https://doi.org/10.1016/S0927-7757\(01\)01019-6](https://doi.org/10.1016/S0927-7757(01)01019-6)
- ⁶ M.M. Khin, A.S. Nair, V.J. Babu, R. Murugan, S. Ramakrishna A review on nanomaterials for environmental remediation, *Energy Environ Sci*, 2012, 5, 8075-8109 <https://doi.org/10.1039/C2EE21818F>
- ⁷ M. A. Aroon, A.F. Ismail, T. Matsuura, MM Montazer-Rahmati, Performance studies of mixed matrix membranes for gas separation: A review, *Sep. Purif. Technol.*, 2010, 75, 229-242 <https://doi.org/10.1016/j.seppur.2010.08.023>
- ⁸ N. Toyoda, T. Yamamoto Dispersion of carbon nanofibers modified with polymer colloids to enhance mechanical properties of PVA nanocomposite film, *Colloids Surf.,A*, 2018, 556, 248-252 <https://doi.org/10.1016/j.colsurfa.2018.03.056>
- ⁹ Z.-H. Dai, T. Li, Y. Gao, J. Xu, Y. Weng, J. He, B.-H. Guo Improved dielectric and energy storage properties of poly(vinyl alcohol) nanocomposites by strengthening interfacial hydrogen-bonding interaction, *Colloids Surf.,A*, 2018, 548, 179-190 <https://www.sciencedirect.com/science/article/pii/S0927775718302450>
- ¹⁰ L. Guod, W. Yuan, Z. Lu, C.M. Li Polymer/nanosilver composite coatings for antibacterial applications, *Colloids Surf. A*, 2013, 439, 69-83 <https://doi.org/10.1016/j.colsurfa.2012.12.029>
- ¹¹ M.S. Selim, H. Yang, S.A.El-Safty, N.A.Fatthallah, M.A. Shenashen, F.Q.Wang, Y. Huang Superhydrophobic coating of silicone/ β -MnO₂ nanorod composite for marine antifouling, *Colloids Surf. A* 2019, 570, 518-530 <https://doi.org/10.1016/j.colsurfa.2019.03.026>

-
- ¹² U.M. Garusinghe, S. Varanasi, V.S.Raghuwanshu, G. Garnier, W. Batchelor Nanocellulose-montmorillonite composites of low water vapour permeability, *Colloids Surf. A* 2018, 540, 233-241 <https://doi.org/10.1016/j.colsurfa.2018.01.010>
- ¹³ M. Gu, X. Li, Y. Cao Optical storage arrays: a perspective for future big data storage, *Light Sci. Appl.* 2014, 3, e177 <https://doi.org/10.1038/lsa.2014.58>
- ¹⁴ W.J. van der Giessen, A.M. Lincoff, R.S. Schwartz, H.M. van Beusekom, P.W. Serruys, D.R. Holmes Jr, S.G. Ellis, E.J. Topol Marked inflammatory sequelae to implantation of biodegradable and nonbiodegradable polymers in porcine coronary arteries, *Circulation*, 1996, 94, 1690-7 <https://doi.org/10.1161/01.CIR.94.7.1690>
- ¹⁵ U. Westedt, M. Wittmar, M. Hellwig, P. Hanefeld, A. Greiner, AK. Schaper, T. Kissel Paclitaxel releasing films consisting of poly(vinyl alcohol)-graft-poly(lactide-co-glycolide) and their potential as biodegradable stent coatings, *J. Controlled Release*, 2006, 111, 235-246 <https://doi.org/10.1016/j.jconrel.2005.12.012>
- ¹⁶ S.C. Dowdy, S. Jiang, X.C. Hou, F. Jin, K.C. Podratz, S.W. Jiang Histone deacetylase inhibitors and paclitaxel cause synergistic effects on apoptosis and microtubule stabilization in papillary serous endometrial cancer cells, *Mol. Cancer Ther.* 2006, 5, 2767-76 <https://doi.org/10.1158/1535-7163.MCT-06-0209>
- ¹⁷ L. Vannozzi, V. Iacovacci, A. Mencias, L. Ricotti Nanocomposite thin films for triggerable drug delivery, *Expert Opin. Drug Deliv.*, 2018, 15, 509-522 <https://doi.org/10.1080/17425247.2018.1451512>
- ¹⁸ D. Quéré, Fluid coating on a fiber, *Annu. Rev. Fluid Mech.*, 1999, 31, 347–384. <https://doi.org/10.1146/annurev.fluid.31.1.347>
- ¹⁹ S. Kwon , W. Kim , H. Kim , S. Choi , B.-C. Park , S.H. Kang , and K. Cheol Choi, High Luminance Fiber-Based Polymer Light-Emitting Devices by a Dip-Coating Method, *Adv. Electron. Mater.* 2015, 1, 1500103 <https://doi.org/10.1002/aelm.201570032>
- ²⁰ X. Tang, X. Yan, Dip-coating for fibrous materials: mechanism, methods and applications *J Sol-Gel Sci Technol.*, 2017, 81, 378–404 <https://doi.org/10.1007/s10971-016-4197-7>
- ²¹ A. Javadi, A. Solouk M. H. Nazarpak, F. Baghee, Surface engineering of titanium-based implants using electrospraying and dip coating methods, *Materials Science & Engineering C*, 2019, 99 620–630. <https://doi.org/10.1016/j.msec.2019.01.027>
- ²² D. Grosso, How to exploit the full potential of the dip-coating process to better control film formation, *J. Mater. Chem.*, 2011, 21, 17033–17038 <https://doi.org/10.1039/C1JM12837J>

-
- ²³ L. Landau and B. Levich, "Dragging of a liquid by a moving plate," *Acta Physico Chimica R.U.S.S.*, 1942, 17, 42-54.
- ²⁴ M. Faustini, B. Louis, P.A. Albouy, M. Kuemmel, D. Grosso, Preparation of Sol–Gel Films by Dip-Coating in Extreme Conditions, *J. Phys. Chem. C*, 2010, 114, 7637-7645
<https://doi.org/10.1021/jp9114755>
- ²⁵ C.J. Brinker, A.J Hurd, G.C Frye, P.R. Schunk, C.S. Ashley Sol-Gel Thin Film Formation, *J. Ceram. Soc. Japan*, 1991, 99, 862-877 <https://doi.org/10.2109/jcersj.99.862>
- ²⁶ S. Roland, C. Guinto Gamys, J. Grosrenaud, S. Boissé, C. Pellerin, R.E. Prud'homme, C. Géraldine Bazuin, Solvent Influence on Thickness, Composition, and Morphology Variation with Dip-Coating Rate in Supramolecular PS-b-P4VP Thin Films, *Macromolecules*, 2015, 48, 4823-4834 <https://pubs.acs.org/doi/abs/10.1021/acs.macromol.5b00847>
- ²⁷ A. Vital, M. Vayer, T. Tillocher, R. Dussart, M. Boufnichel, C. Sinturel Morphology control in thin films of PS:PLA homopolymer blends by dip-coating deposition, *Appl. Surf. Sci.*, 2017, 393, 127-133 <https://doi.org/10.1016/j.apsusc.2016.09.151>
- ²⁸ S. Roland, R.E.Prud'homme, C.G. Bazuin Morphology, Thickness, and Composition Evolution in Supramolecular Block Copolymer Films over a Wide Range of Dip-Coating Rates, *ACS Macro Lett.* 2012, 1, 973-976
<https://pubs.acs.org/doi/full/10.1021/mz3003165?src=recsys>
- ²⁹ C. Loussert, F. Doumenc, J.-B. Salmon, V. S. Nikolayev, B. Guerrier Role of vapor mass transfer in flow coating of colloidal dispersions in the evaporative regime *Langmuir*, 2017, 33, 14078-14086 <https://pubs.acs.org/doi/abs/10.1021/acs.langmuir.7b03297>
- ³⁰ R.D Deegan, O. Bakajin, T.F Dupont, G. Huber, S.R Nagel, T.A Witten Contact line deposits in an evaporating drop, *Phys. Rev E*, 2000, 62, 756-65
<https://doi.org/10.1103/PhysRevE.62.756>
- ³¹ R. D. Deegan, O. Bakajin, T. F. Dupont, G. Huber, S. R. Nagel, T. A. Witten, Capillary flow as the cause of ring stains from dried liquid drops, *Nature*, 1997, 389, 827-829
<https://doi.org/10.1038/39827>
- ³² J. Huang, R. Fan, S. Connor, P. Yang One-Step Patterning of Aligned Nanowire Arrays by Programmed Dip Coating, *Angew. Chem. Int. Ed. Engl.* 2007, 46, 2414–2417
<https://doi.org/10.1002/anie.200604789>
- ³³ M. Ghosh, F. Fan, K.J. Stebe Spontaneous Pattern Formation by Dip Coating of Colloidal Suspensions on Homogeneous Surfaces *Langmuir* 2007, 23, 2180–2183
<https://doi.org/10.1021/la062150e>

-
- ³⁴ B.M. Dincau, M.Z. Bazant, E. Dressaire, A. Sauret, Capillary Sorting of Particles by Dip Coating, *Phys. Rev. Appl.*, 2019, 12, 011001
<https://doi.org/10.1103/PhysRevApplied.12.011001>
- ³⁵ A. Sauret, A. Gans, B. Colnet, G. Saingier, M. Z. Bazant, E. Dressaire Capillary filtering of particles during dip coating, *Phys. Rev. Fluids*. 2019, 4, 054303
<https://doi.org/10.1103/PhysRevFluids.4.054303>
- ³⁶ D. S. Patil, J. S. Shaikh, S. A. Pawar, R. S. Devan, Y. R. Ma, A. V. Moholkar, J. H. Kim, R. S. Kalubarme, C. J. Park, P. S. Patil, Investigations on silver/polyaniline electrodes for electrochemical supercapacitors *Phys. Chem. Chem. Phys.* ,2012,14,11886–11895
<https://doi.org/10.1039/C2CP41757J>
- ³⁷ S. Sugumaran, C.S. Bellan Transparent nano composite PVA-TiO₂ and PMMA-TiO₂ thin films: Optical and dielectric properties, *Optik* 2014, 125, 5128-5133
<https://doi.org/10.1016/j.ijleo.2014.04.077>
- ³⁸ M. Catauro, F. Papale, F. Bollino Characterization and biological properties of TiO₂/PCL hybrid layers prepared via sol–gel dip coating for surface modification of titanium implants *J. Non-Cryst. Solids* 2015, 415, 9-15 <https://doi.org/10.1016/j.jnoncrysol.2014.12.008>
- ³⁹ I. Galeska, T.-K. Kim, S.D. Patil, U. Bhardwaj, D. Chattopadhyay, F. Papadimitrakopoulos, D.J. Burgess Controlled release of dexamethasone from PLGA microspheres embedded within polyacid-containing PVA hydrogels, *AAPS J.* 2005, 7, 231–240 <https://dx.doi.org/10.1208%2Faapsj070122>
- ⁴⁰ D.B. Tada, S. Singh, D. Nagesha, E. Jost, C.O. Levy, E. Gultepe, R. Cormack, G.M. Makrigiorgos, S. Sridhar Chitosan Film Containing Poly(D,L-Lactic-Co-Glycolic Acid) Nanoparticles: A Platform for Localized Dual-Drug Release, *Pharm. Res.* 2010, 27, 1738–1745 <https://doi.org/10.1007/s11095-010-0176-9>
- ⁴¹ T. C. Dos Santos, N. Rescignano, L. Boff, F.H. Reginatto, C.M.O. Simões, A.M. de Campos, C.U. Mijangos Manufacture and characterization of chitosan/PLGA nanoparticles nanocomposite buccal films, *Carbohydr. Polym.* 2017, 173, 638-644
<https://doi.org/10.1016/j.carbpol.2017.06.014>
- ⁴² F. Tewes, E. Munnier, B. Antoon, L. Ngaboni Okassa, S. Cohen-Jonathan, H. Marchais, L. Douziech-Eyrolles, M. Soucé, P. Dubois, I. Chourpa Comparative study of doxorubicin-loaded poly(lactide-co-glycolide) nanoparticles prepared by single and double emulsion methods, *Eur. J. Pharm. Biopharm.*, 2007, 66, 488-492
<https://doi.org/10.1016/j.ejpb.2007.02.016>
- ⁴³ C.J. Brinker, Dip coating, in: T. Schneller, R. Waser, M. Kosec, D. Payne (Eds.), *Chemical Solution Deposition of Functional Oxide Thin Films*, Springer, Vienna, 2013, pp. 233–261.

⁴⁴ G. Berteloot, A. Daerr, F. Lequeux, L. Limat Dip coating with colloids and evaporation Chemical Engineering and Processing 2013, 68, 69–73
<http://dx.doi.org/10.1016/j.cep.2012.09.001>

⁴⁵ M. Vayer, A. Pineau, F. Warmont, M. Roulet, C. Sinturel, Constrained crystallization of poly(L-lactic acid) in thin films prepared by dip coating Eur. Polym. J., 2018, 101, 332-340
<https://doi.org/10.1016/j.eurpolymj.2018.03.006>

⁴⁶ N.A. Peppas, P. J. Hansen Crystallization kinetics of poly(vinyl alcohol), J. Appl. Polym. Sci. 1982, 27, 4787-4797 <https://doi.org/10.1002/app.1982.070271223>

⁴⁷ A. Gans, E. Dressaire, B. Colnet, G. Saingier, M. Z. Bazant and A. Sauret, Dip-coating of suspensions, Soft Matter, 2019, 15, 252-261.
<https://doi.org/10.1039/c8sm01785a>